IAHR AIRH

Journal of Hydraulic Research Vol. 46, No. 1 (2008), pp. 65–72

Turbulence and cavity recirculation in air–water skimming flows on a stepped spillway

Turbulence et cavité de recirculation dans les écoulements d'écume air-eau sur un déversoir en gradins

C.A. GONZALEZ, *Division of Civil Engineering, The University of Queensland, Brisbane QLD 4072, Australia.*

H. CHANSON, IAHR Member, *Division of Civil Engineering, The University of Queensland, Brisbane QLD 4072, Australia.*
Tel.: (617)33653516; fax: (617)33654599; e-mail: h.chanson@uq.edu.au

ABSTRACT
Current expertise in air–water turbulent flows on stepped chutes is limited mostly to laboratory experiments at low to moderate Reynolds numbers on chutes with flat horizontal steps. In this study, highly turbulent air–water flows skimming down a large-size stepped chute were investigated with a 1V:2.5H slope. For some experiments, the cavity recirculation was controlled using triangular vanes, or longitudinal ribs, to enhance the interactions between the skimming flow and cavity recirculating region. New experiments were performed with seven configurations. The results demonstrated the strong influence of the vanes on the cavity recirculation patterns and on the air–water flow properties. An increase in flow resistance was observed consistently with maximum rate of energy dissipation achieved with vanes placed in a zigzag pattern.

RÉSUMÉ
L'expertise courante des écoulements turbulents air-eau sur les déversoirs en gradins est limitée la plupart du temps à des expériences en laboratoire faites avec des nombres de Reynolds faibles à modérés, et sur des déversoirs à marches plates et horizontales. Dans cette étude, des écoulements fortement turbulents de mélange air-eau dévalant une grande chute en gradins ont été étudiés avec une pente de 1V:2.5H. Dans certaines expériences, la cavité de recirculation était contrôlée au moyen de palettes triangulaires, ou de nervures longitudinales, permettant d'augmenter les interactions entre l'écoulement d'écume et la zone de recirculation. De nouvelles expériences ont été exécutées avec sept configurations différentes. Les résultats ont montré la forte influence des palettes sur les types de recirculation et sur les propriétés de l'écoulement air-eau. On a observé une augmentation de la résistance d'écoulement en rapport avec un taux maximum de dissipation d'énergie lorsque les palettes sont placées dans une disposition en zigzag.

Keywords: Air entrainment, cavity recirculation, flow resistance, physical modelling, skimming flows, turbulence, stepped spillways.

1 Introduction

Numerous studies of stepped spillway flows were conducted with different approaches over the past nearly 40 years. Pertinent reviews include Chanson (2001), Mossa *et al.* (2004) and Ohtsu *et al.* (2004). Only a limited number of published papers refer to highly turbulent flows associated with strong free-surface aeration (e.g. Chanson and Toombes, 2002; Boes and Hager, 2003; Yasuda and Chanson, 2003). The stepped chute design is common for overflow spillways of gravity and embankment dams. Most structures are designed with flat horizontal steps but some included devices to enhance energy dissipation (Andre *et al.*, 2004; Chanson and Gonzalez, 2004). Modern stepped spillways are designed to operate with a skimming flow regime. In a skimming flow, the waters flow down the stepped channel as a coherent stream skimming over the pseudo-bottom zones formed by step edges (Rajaratnam, 1990; Chamani and Rajaratnam, 1999). Beneath, the cavity recirculation is maintained through the transmission of momentum from the main stream (Fig. 1). Orlandi *et al.* (2006) performed a pertinent numerical study with square and triangular cavities. Their results showed that the normal velocity fluctuations along the pseudo-bottom formed by the step edges (i.e. $y = 0$, Fig. 1) would be the driving mechanism of the cavity vorticity field.

There may be some analogy between the skimming flow over stepped spillways and skimming flows above large roughness elements, including boundary layer flows past d-type roughness (e.g. Chanson *et al.*, 2002; Djenidi *et al.*, 1999). The d-type roughness consists of closely spaced rectangular cavities. A pertinent study by Mochizuki *et al.* (1996) investigated some turbulent boundary layer flow past square cavities with thin longitudinal ribs. Despite conflicting interpretations of their data, their experiments demonstrated some turbulence manipulation by interfering with the recirculation vortices.

This paper presents the result of a systematic investigation into the effects of several vane configurations on the cavity recirculation and on the skimming flow properties. The experiments were conducted in a large stepped channel operating with Reynolds numbers between 4 E+5 and 8 E+5. One configuration had flat horizontal steps while six others were equipped with

Revision received March 21, 2007/Open for discussion until August 31, 2008.

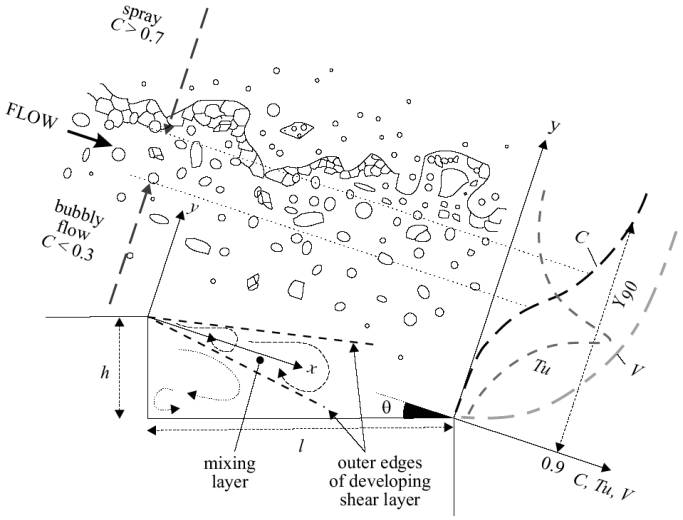

Figure 1 Sketch of skimming flows down a moderate-slope stepped spillway.

vane arrangements (Fig. 2; Table 1). The interactions between free surface and cavity recirculation, turbulence manipulation and flow resistance were systematically investigated for several discharges.

2 Experimental facilities

The new experiments were conducted at the University of Queensland in a 3.3 m long 1 m wide 1V:2.5H slope chute with flow rates ranging from 0.10 to 0.19 m^3/s corresponding to a skimming flow regime (Table 1). The water supply pump was controlled by an adjustable frequency AC motor drive which enabled for an accurate control of the closed circuit system. The waters were fed from a large basin (1.5 m deep, surface area 6.8 m × 4.8 m) leading to a sidewall convergent with a 4.8:1 contraction ratio to minimize the inflow turbulence. The test section consisted of a 1 m wide 0.62 m long broad-crested weir with upstream rounded corner followed by 10 identical steps ($h = 0.1$ m, $l = 0.25$ m) made of marine ply. The stepped chute ($\theta = 21.8°$) had perspex sidewalls (Fig. 2b) and it ended in a horizontal concrete-invert canal leading to a dissipation pit.

2.1 Cavity configurations

In the present study, seven-stepped geometries were tested systematically with several flow rates (Table 1; Fig. 2). The first configuration had 10 identical flat horizontal steps (Configuration 1). This first geometry was similar to that studied by Chanson and Toombes (2002). Experimental observations highlighted the three-dimensional nature of recirculation vortices in the step cavities. In absence of vanes, three to four cavity recirculation cells were observed across the 1 m wide channel. These recirculation vortices were believed to be related to longitudinal (streamwise) coherent structures in the mainstream flow.

For the rest of the configurations (second to seventh configurations), some vanes or longitudinal ribs were placed across the step cavity from steps 2 to 10 as illustrated in Fig. 2. The triangular vanes (0.1 m × 0.25 m) were made of aluminium, although a few were made in perspex for flow visualization next to the wall. The vanes did not interfere with the free-stream (Fig. 2). The second and fourth configurations had, respectively, 3 and 7 vanes placed in line. The third and fifth configurations had, respectively, 3 (or 4) and 7 (or 8) vanes placed in zigzag (or staggered). The sixth configurations had 7 vanes per step set in line every two steps, while the seventh configuration consisted of 7 (or 8) vanes per step set in a zigzag pattern every two steps.

For each configuration, the air–water flow measurements were repeated systematically at each step edge downstream of the inception point of free-surface aeration and at several longitudinal positions between adjacent step edges (i.e. above recirculation cavity), as well as at several transverse positions for several flow rates. A total of more than 240 vertical profiles were recorded with a minimum of 25 measurement points per profile. Further details on the experiments were reported in Gonzalez (2005).

2.2 Instrumentation and data processing

Clear-water flow depths were measured with a point gauge. The flow rate was deduced from the measured upstream head above crest after a detailed *in situ* calibration (Gonzalez, 2005). The air–water flow properties were recorded with a double-tip conductivity probe (Ø = 0.025 mm) previously used by Chanson and Toombes (2002), Toombes (2002), Yasuda and Chanson (2003) and Gonzalez and Chanson (2004a). The probe sensors were aligned in the flow direction. The leading tip had a small frontal area (i.e. 0.05 mm^2) and the trailing tip was laterally offset by 1 mm to avoid wake disturbance from the first tip. An air bubble detector (UQ82.518) excited the probe. Its output signal was scanned at 20 kHz for 20 s per probe tip. The translation of the probes in the direction normal to the flow was controlled by a fine adjustment travelling mechanism connected to a Mitutoyo™ digimatic scale unit. The error on the vertical position of the probe was less than 0.2 mm. The accuracy on the longitudinal probe position was estimated as $\Delta x < \pm 0.5$ cm. The accuracy on the transverse position of the probe was less than 1 mm. Flow visualizations were conducted with high-shutter speed digital still and video cameras.

The basic probe outputs were the void fraction, velocity, turbulence intensity and air–water chord size distributions. The void fraction C is the proportion of time that the probe tip is in the air. With a dual-tip probe design, the velocity measurement is based upon the successive detection of air–water interfaces by the two tips. Herein the longitudinal velocity V was calculated using a cross-correlation technique (e.g. Crowe *et al.*, 1998). The turbulence level Tu (in the longitudinal direction) was derived from the broadening of the cross-correlation function compared to the auto-correlation function (Chanson and Toombes, 2002). Physically, a thin, narrow cross-correlation function corresponds to little fluctuations in interfacial velocity, hence a small turbulence level. The turbulence level Tu is not a point measurement but some spatial average between the two probe sensors. For low volume fractions, it is equal to the turbulence intensity u'/V, where

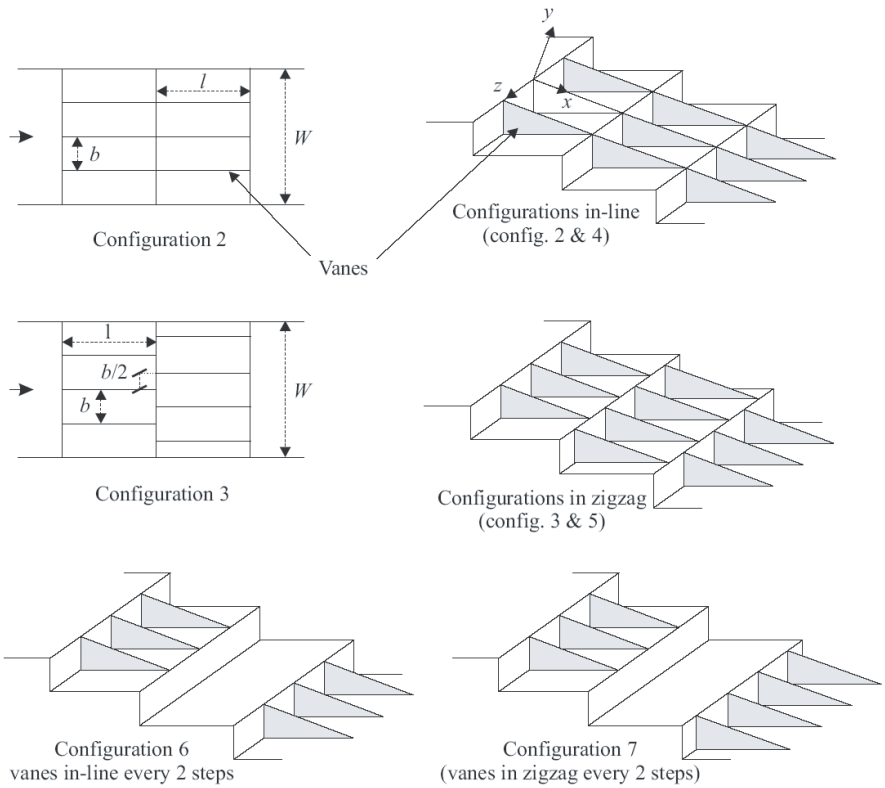

(a)

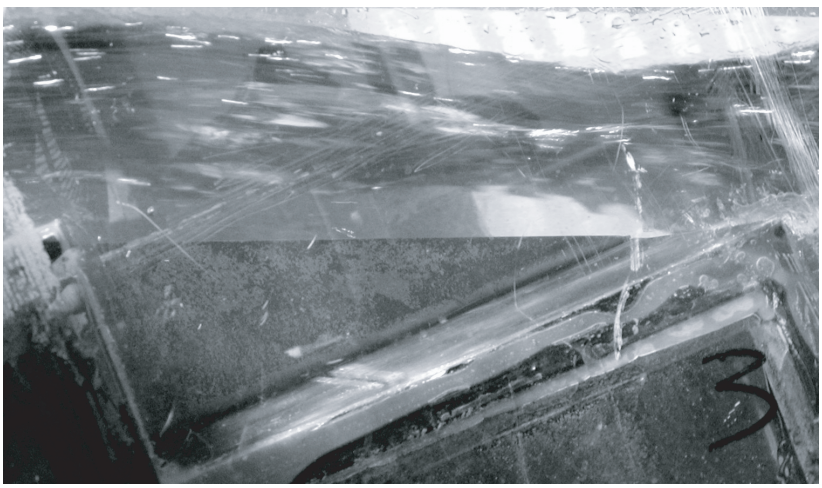

(b)

Figure 2 Cavity configurations. (a) Sketch of the vane configurations. (b) Photograph of the stepped chute (Configuration 4) in operation for $d_c/h = 1.25$ (flow from left to right): The triangular vanes are visible immediately upstream of the inception point of free-surface aeration.

Table 1 Detailed air–water flow investigations in skimming flows on the 22° stepped chute

Reference	θ(○)	q_w(m^2/s)	h(m)	Re	Instrumentation	Geometry
Present Study	21.8	0.10 to 0.19	0.1	4E+5 to 8E+5	Double-tip conductivity probe (Ø = 0.025 mm)	$L = 3.3$ m. $W = 1$ m. Uncontrolled broad-crest
Configuration 1						$b = W = 1$ m (no vane).
Configuration 2						$b = W/4 = 0.25$ m (3 vanes in line)
Configuration 3						$b = W/4 = 0.25$ m (3 or 4 vanes in zigzag)
Configuration 4						$b = W/8 = 0.125$ m (7 vanes in line)
Configuration 5						$b = W/8 = 0.125$ m (7 or 8 vanes in zigzag)
Configuration 6						$b = W/8 = 0.125$ m (7 vanes in line, every 2 steps)
Configuration 7						$b = W/8 = 0.125$ m (7 or 8 vanes in zigzag, every two steps)

Note: Re: Reynolds number in terms of the hydraulic diameter.

u' is the standard deviation of the longitudinal velocity component. Chord sizes were calculated from the raw probe signal outputs.

3 Flow observations

The skimming flows looked similar to some self-aerated flows down smooth chutes. At the upstream end, the flow was smooth and transparent. When the outer edge of the developing bottom boundary layer reached the free surface, turbulence induced strong aeration. Downstream of the point of inception of free-surface aeration, the air–water flow became fully developed and strong exchanges of air–water and momentum occurred between the main stream and the atmosphere. Intense cavity recirculation was observed also below the pseudo-invert formed by the step edges. The air–water flow mixture consisted of a bubbly region ($C < 30\%$), a spray region ($C > 70\%$) and an intermediate zone in between (Fig. 1). Some three-dimensional cavity vortices developed beneath the pseudo-bottom formed by the step edges (Matos, 2001) and the recirculation was maintained through the transmission of momentum from the main stream. Some small-scale vorticity was also generated at the corner of the steps. Skimming flows were characterised by very significant form losses and momentum transfer from the main stream to the recirculation zones as demonstrated by Gonzalez and Chanson (2004a) with a 16° slope angle.

Observations through the sidewall showed some effects of the vanes on cavity recirculation. Vanes appeared to be subjected to strong pressure and shear forces. Fluctuations seemed to be of the same period and in phase with cavity fluid ejections discussed by Chanson *et al.* (2002). Some longitudinal free-surface troughs were also observed above the vanes, possibly associated with wakes and quasi-coherent low speed streaks immediately above each vane.

4 Distributions of air–water flow properties

A detailed comparison of the distributions of air–water flow properties was conducted for the stepped configurations with and without vanes. The comparison was based upon experimental data measured at three transverse locations $z/b = 0$, 0.25 and 0.5, where z is the transverse distance from the channel centreline and b is the transverse spacing between vanes (Fig. 2). All the results were compared with the data for the stepped geometry without vanes (Configuration 1). Figure 3 presents typical results in terms of dimensionless distributions of air concentration C and velocity V/V_{90} for Configurations 1, 4, 5, 6 and 7 at step edge 9 and $z/b = 0.25$, where y is the distance normal to the pseudo-bottom formed by the step edges, Y_{90} is the distance where $C = 0.90$ and V_{90} is the air–water flow velocity at $y = Y_{90}$.

The void fraction distributions, including the data presented in Fig. 3, suggested some negligible effects of the vanes on the void fraction distributions and on the rate of air entrainment. At step edges, the distributions of air concentration compared favourably with an analytical solution of the air bubble diffusion equation:

$$C = 1 - \tanh^2\left(K' - \frac{y'}{2 \times D_0} + \frac{\left(y' - \frac{1}{3}\right)^3}{3 \times D_0}\right) \quad (1)$$

where $y' = y/Y_{90}$ (Chanson and Toombes, 2002). D_0 and K' are dimensionless functions of the mean air concentration C_{mean}:

$$K' = 0.327 + \frac{1}{2 \times D_0} - \frac{8}{81 \times D_0} \quad (2)$$

$$D_0 = 0.0117 - 0.277 \times Ln(1 - 1.258 \times C_{mean}) \quad C_{mean} < 0.79 \quad (3)$$

with

$$C_{mean} = \int_0^1 C \times dy' \quad (4)$$

Equation (1) is compared with the data in Fig. 3.

The velocity measurements at all transverse positions for each vane configuration showed a strong effect of the vanes on the flow for $y/Y_{90} < 0.5$ to 0.7. In absence of vanes, the velocity distribution at each edge followed closely a power law for $y' = 1$ and a quasi-uniform profile above:

$$\frac{V}{V_{90}} = y'^{1/N} \quad 0 \leq y' \leq 1 \quad (5)$$

$$\frac{V}{V_{90}} = 1 \qquad 1 \leq y' \quad (6)$$

Equation (5) is shown in Fig. 3 assuming $N = 7$.

In presence of vanes, a velocity defect region was observed above the longitudinal ribs, suggesting a developing wake region above each vane (Fig. 3). The results demonstrated that the effect of the vanes was not limited to the cavity flow but extended into the mainstream. Figure 4 presents some dimensionless distributions of velocity V/V_{90} and turbulence level Tu measured between step edges. The data include the configurations 1, 4, 5, 6 and 7. All the data for configurations with vanes were measured at $z/b = 0.25$. The experimental results hinted that the streamwise effect of vanes was limited to one downstream cavity, because no noticeable difference in terms of velocity and turbulence level distributions was observed between Configurations 1, 6 and 7 despite the presence of vanes every two steps in Configurations 6 and 7.

The turbulence level distributions showed high values for all investigated flow conditions. For the configurations with vanes, the results showed consistently higher turbulence levels than in absence of vanes (e.g. Fig. 4). The findings suggested that the presence of vanes induced an increase of turbulence by about 40%. The maximum turbulence levels were observed for Configurations 3 and 5 (i.e. with vanes in zigzag).

In the highly turbulent skimming flows, the probability distribution functions (PDFs) of bubble chord sizes were systematically analysed for each configuration in the bubbly flow region ($C < 0.3$) while the drop size distributions were studied in the spray region ($C > 0.7$). Figure 5 presents some typical bubbly flow results for identical configurations. The data were

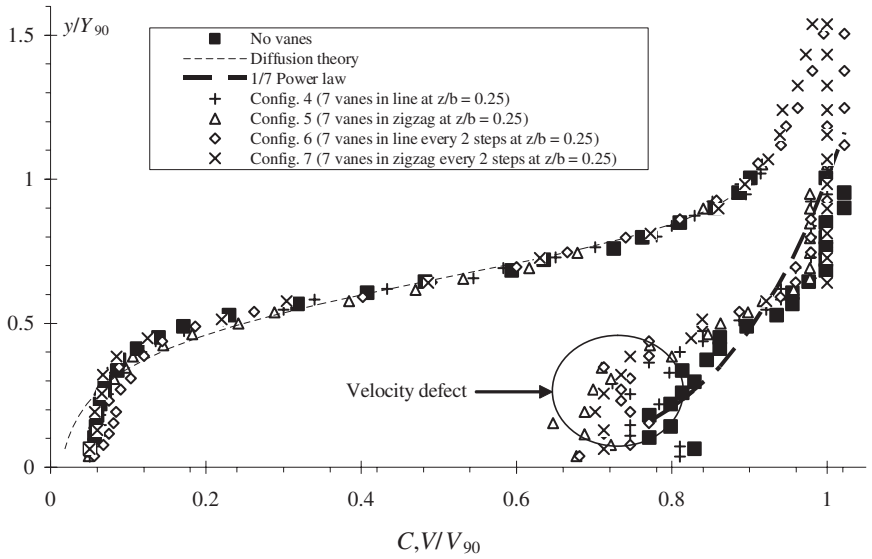

Figure 3 Dimensionless distributions of void fraction and velocity at step edge 9 ($d_c/h = 1.4$, Re = 6.5 E+5): comparison between Eqs (1) and (5) and experimental data for the configuration 1 (no vane) and configurations 4–7 (7 vanes) at $z/b = 0.25$.

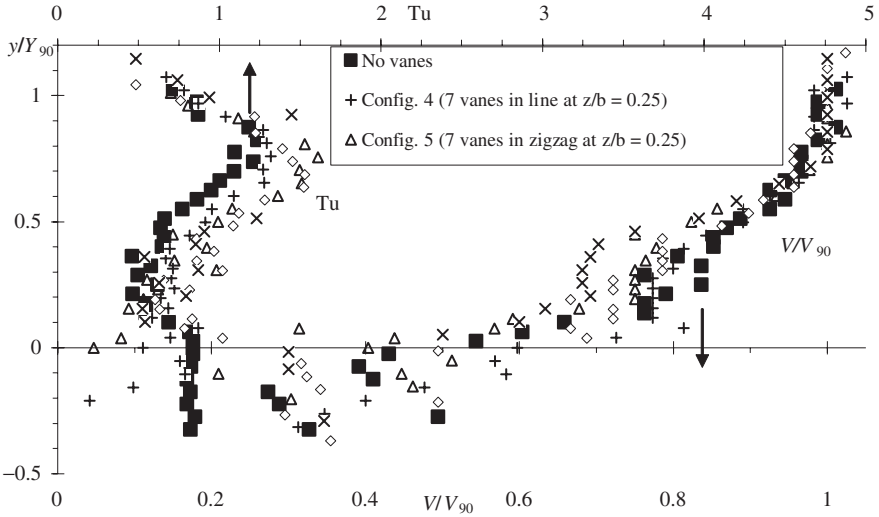

Figure 4 Dimensionless distributions of velocity and turbulence intensity at one quarter of the distance between step edges 9 and 10 ($d_c/h = 1.4$, Re = 6.5 E+5): comparison between configuration 1 (no vane) and configurations 4–7 (7 vanes) at $z/b = 0.25$ and $x/\sqrt{h^2 + l^2} = 0.25$.

measured between step edges at some locations below (Fig. 5a) and above (Fig. 5b) the pseudo-bottom with similar void fractions. In Fig. 5, each legend gives further details of the local air–water flow properties including the number of detected bubbles in the 20 s record. Overall the results demonstrated a greater number of bubbles detected in the mainstream ($y > 0$) and a broader range of bubble sizes than at locations below the pseudo-bottom for an identical void fraction. For example, in Fig. 5, the amount of bubbles which were detected in the mainstream (Fig. 5b) was nearly 5 times that detected in the recirculation region (Fig. 5a) for locations with similar void fractions. Further the results suggested that the presence of vanes and the vane configurations had little effects on the air–water flow structures. For example, in Fig. 5, very few difference is seen between the Configurations 1, 2 and 3 (no vane, 3 vanes in line and 3 vanes in zigzag, respectively).

5 Rate of energy dissipation and flow resistance

Downstream of the inception point of free-surface aeration, the rate of energy dissipation may be expressed in terms of the average friction factor. Herein the flow resistance was estimated from the friction slope S_f calculated at $z/b = 0$ (above vanes), 0.25 and 0.5 for all the configurations, using the approach of Chanson *et al.* (2002). The friction slope is the total head line gradient and it was calculated from the air–water flow properties. The results are presented in terms of the Darcy–Weisbach friction factor f_e in Table 2. The friction factor was calculated as:

$$f_e = \frac{8 \times g}{q_w^2} \times \left(\int_{y=0}^{Y_{90}} (1 - C) \times dy \right)^3 \times S_f \quad (7)$$

where q_w is the water discharge per unit width and g is the gravity constant. The friction factor f_e is a longitudinally averaged

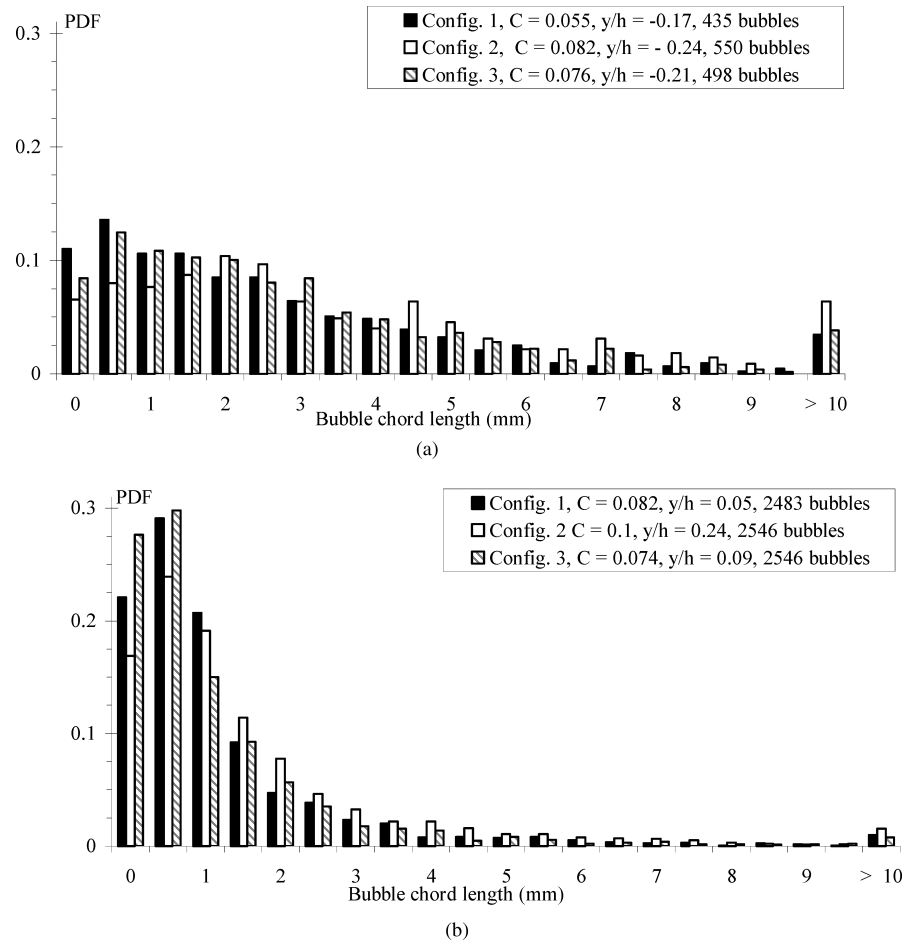

Figure 5 Probability distributions functions of air bubble chord for $C < 0.3$ and $d_c/h = 1.4$ between step edges 9 and 10 at $x/\sqrt{h^2 + l^2} = 0.25$ and $z/b = 0.25$. (a) Measurements below the pseudo-bottom ($y' < 0$). (b) Measurements in the free-stream flow above the pseudo-bottom ($y' > 0$).

friction factor, and the measurements were conducted at three dimensionless transverse locations $z/b = 0$, 0.25 and 0.5 (Table 2).

For each configuration with vanes, the results were averaged transversally to yield an equivalent friction factor $\overline{f_e}$ of the whole chute defined as:

$$\overline{f_e} = \frac{1}{W} \times \int_{-W/2}^{+W/2} \left[\frac{8 \times g}{q_w^2} \times \left(\int_{y=0}^{y_{90}} (1 - C) \times dy \right)^3 \times S_f \right] \times dz \quad (8)$$

Table 2 Flow resistance estimates in air–water skimming flows at several transverse locations($z/b = 0$, 0.25, 0.5)

d_c/h	f_e								
	Configuration 1 no vane	Configuration 2 3 vanes in line			Configuration 3 3 vanes in zigzag		Configuration 4 7 vanes in line		
		$z/b = 0$	$z/b = 0.25$	$z/b = 0.5$	$z/b = 0.25$	$z/b = 0.5$	$z/b = 0$	$z/b = 0.25$	$z/b = 0.5$
1.1	0.169	0.238	0.167	0.186	0.141	0.212	—	0.174	0.170
1.25	0.176	0.236	0.186	0.173	0.151	0.287	—	0.170	0.176
1.4	0.0924	0.311	0.145	0.133	0.207	0.288	0.281	0.165	0.166
1.5	0.211	0.271	0.191	0.258	0.225	0.227	—	0.170	0.163

d_c/h	f_e						
	Configuration 5 7 vanes in zigzag		Configuration 6 7 vanes in line every 2 steps			Configuration 7 7 vanes in zigzag every 2 steps	
	$z/b = 0.25$	$z/b = 0.5$	$z/b = 0$	$z/b = 0.25$	$z/b = 0.5$	$z/b = 0.25$	$z/b = 0.5$
1.1	0.180	0.238	0.216	0.177	0.181	0.165	0.2057
1.25	0.205	0.3112	0.258	0.167	0.191	0.120	0.236
1.4	0.211	0.249	0.266	0.163	0.160	0.136	0.231
1.5	0.215	0.170	0.373	0.121	0.163	0.207	0.346

where z is the transverse distance measured from the centreline and W is the chute width. Equation (8) was calculated based upon measurements at three locations ($z = 0$, $z = b/4$ and $z = b/2$) relative to the rib positions that were transposed by simple theory of superposition. For example, the results at $z = 0$ are also valid at $z = b$, $2 \times b, \ldots$, while the results at $z = +b/4$ are also valid $z = -b/4$ and $z = 3 \times b/4$. Some measurements were conducted at five transverse locations and the results validated the superposition method.

The equivalent friction factor $\overline{f_e}$ is a "double-averaged" friction factor, in the sense that it is averaged in both longitudinal and transverse directions. The experimental measurements yielded equivalent Darcy–Weisbach friction factors $\overline{f_e}$ of 0.16, 0.21, 0.21 and 0.20 in average for no vane, 3 and 7 vanes in line, and 7 vanes in line every two steps, respectively (Configurations 1, 2, 4, 6). The results implied further friction factors of $\overline{f_e} = 0.22$, 0.22 and 0.21 in average for 3 and 7 vanes in zigzag, and 7 vanes in zigzag every two steps, respectively (Configurations 3, 5, 7).

Basically the findings suggested consistently that the presence of vanes increased the flow resistance and the rate of energy dissipation for the investigated flow conditions. Maximum values of equivalent Darcy–Weisbach friction factors were observed for the configurations with vanes in zigzag (Configurations 3 and 5). It is thought that the staggered configurations provided a lesser degree of sheltering by the upstream rib elements. The results for the configuration 6 and 7 (vanes every 2 steps) indicated systematically a lower flow resistance for these configurations than that with the other configurations with vanes.

6 Discussion

In absence of vanes, the present observations showed the existence of three to four recirculation cells across the 1 m wide cavities. The presence of longitudinal ribs modified the cavity recirculation process. The vanes prevented the transverse development of large-scale turbulence in each cavity. It is believed that the inhibition of large transverse vortical structures was associated with some enhanced vertical mixing between the recirculation zones and mainstream. It suggested a modification of the mixing layer developing downstream of each step edge (Fig. 1), with a greater rate of expansion and larger transfer of momentum from the free-stream to the cavity flow in presence of triangular ribs. The turbulent mixing enhancement was further associated with the development of streamwise coherent vortices in the main stream. Some greater vertical mixing was also associated with a stronger spray generation in the configurations with vanes. Experimental data showed consistently that the dimensionless water flux for $0.90 \leq C \leq 0.99$ doubled in presence of longitudinal vanes (Gonzalez, 2005).

7 Conclusion

The turbulent and cavity recirculation processes were investigated systematically in skimming flows down a stepped chute. The results were obtained in a large-size facility operating at large Reynolds numbers to minimize potential scale effects discussed thoroughly by Boes (2000) and Gonzalez and Chanson (2004b). Several step cavity configurations were systematically tested and compared with the classical flat-step geometry. These consisted of a number of triangular vane arrangements (Fig. 2; Table 1). Detailed air–water flow measurements were performed downstream of the inception of free-surface aeration. The experimental results demonstrated that the triangular vanes influenced the air–water flow properties in both the mainstream and recirculating regions. The results showed that maximum flow resistance was observed for the configurations with vanes placed in a zigzag pattern. It is believed that the presence of ribs prevented the development of large-scale transverse vortices in the cavity, and enhanced the vertical momentum mixing between the recirculation zones and the skimming flow.

Based upon the present results, it is hypothesized that greatest interfacial aeration and air–water transfer rates might be achieved with vane configurations in zigzag placed at each step. It is also suggested that more intricate geometries (e.g. vanes in zigzag every two steps) will not enhance further the flow resistance. This study provides some new information on the complex air–water structure of highly turbulent skimming flows and it hints some basic mechanisms of energy dissipation enhancements for stepped spillway design.

Acknowledgments

The authors acknowledge the helpful comments of Dr John Macintosh (Water Solutions), and the technical assistance of Graham Illidge and Clive Booth (The University of Queensland). The first author thanks the financial support of the National Council for Science and Technology of Mexico (CONACYT).

Notation

b = Transverse spacing (m) between longitudinal ribs
C = Void fraction
C_{mean} = Depth-averaged void fraction defined in terms of Y_{90}: $C_{mean} = 1 - d/Y_{90}$
D_H = Equivalent pipe diameter or hydraulic diameter (m)
D' = Dimensionless air bubble diffusivity
d = Equivalent clear water flow depth defined as: $d = \int_{y=0}^{Y_{90}} (1 - C) \times dy$
d_c = Critical flow depth (m)
f_e = Equivalent Darcy–Weisbach friction factor in air–water skimming flows
$\overline{f_e}$ = Transverse-averaged Darcy–Weisbach friction factor of the stepped chute
g = Gravity constant: $g = 9.80\ m/s^2$ in Brisbane, Australia
h = Vertical step height (m)
K' = Dimensionless integration constant
L = Chute length (m)
l = Horizontal step length (m)
q_w = Water discharge per unit width (m^2/s)
Re Reynolds number defined in terms of the hydraulic diameter: $Re = \rho_w \times V \times D_H/\mu_w$

S_f = Friction slope
Tu = Turbulence intensity: $Tu = u'/V$
u' = Root mean square of longitudinal component of longitudinal air–water interfacial velocity (m/s)
x = Longitudinal coordinate (m) in the flow direction
y = Distance (m) normal to the pseudo-bottom formed by the step edges
y' = Dimensionless distance: $y' = y/Y_{90}$
z = Transverse distance (m) from the channel centreline
V = Longitudinal air–water interfacial velocity (m/s)
V_{90} = Characteristic air–water interfacial velocity (m/s) at $y = Y_{90}$
W = Chute width (m)
Y_{90} = Characteristic distance where $C = 0.90$
μ_w = Dynamic viscosity of water (Pa.s)
θ = Angle between the pseudo-bottom formed by the step edges and the horizontal
ρ_w = Water density (kg/m^3)
Ø = Diameter (m)

References

1. ANDRE, S., BOILLAT, J.L., SCHLEISS, A.J. and MATOS, J. (2004). "Energy Dissipation and Hydrodynamic Forces of Aerated Flow over Macro-Roughness Linings for Overtopped Embankment Dams". *Proceedings of the International Conference on Hydraulics of Dams and River Structures*, Tehran, Iran, Balkema Publ., The Netherlands, pp. 189–196.
2. BOES, R.M. (2000). "Scale Effects in Modelling Two-Phase Stepped Spillway Flow". *International Workshop on Hydraulics of Stepped Spillways*, Zürich, Switzerland, Balkema Publ., pp. 53–60.
3. BOES, R.M. and HAGER, W.H. (2003). "Two-Phase Flow Characteristics of Stepped Spillways". *J. Hydraul. Engg. ASCE* 129(9), 661–670. Discussion: 131(5), 419–429.
4. CHAMANI, M.R. and RAJARATNAM, N. (1999). "Characteristics of Skimming Flow Over Stepped Spillways". *J. Hydraul. Engg. ASCE* 125(4), 361–368.
5. CHANSON, H. (2001). *The Hydraulics of Stepped Chutes and Spillways*. Balkema, Lisse, The Netherlands, 418 pp.
6. CHANSON, H. and GONZALEZ, C.A. (2004). "Stepped Spillways for Embankment Dams: Review, Progress and Development in Overflow Hydraulics". *Proceedings of the International Conference on Hydraulics of Dams and River Structures*, Tehran, Iran, Balkema Publ., The Netherlands, 287–294.
7. CHANSON, H. and TOOMBES, L. (2002). "Air–Water Flows Down Stepped Chutes: Turbulence and Flow Structure Observations". *Intl. J. Multiphase Flow* 27(11), 1737–1761.
8. CHANSON, H., YASUDA, Y. and OHTSU, I. (2002). "Flow Resistance in Skimming Flows and Its Modelling". *Can. J. Civ. Engg.* 29(6), 809–819.
9. CROWE, C., SOMMERFIELD, M. and TSUJI, Y. (1998). *Multiphase Flows with Droplets and Particles*. CRC Press, Boca Raton, USA, 471 pp.
10. DJENIDI, L., ELAVASARAN, R. and ANTONIA, R.A. (1999). "The Turbulent Boundary Layer Over Transverse Square Cavities". *J. Fluid Mech.* 395, 271–294.
11. GONZALEZ, C.A. (2005). "An Experimental Study of Free-Surface Aeration on Embankment Stepped Chutes". PhD Thesis, Department of Civil Engineering, University of Queensland, Brisbane, Australia.
12. GONZALEZ, C.A. and CHANSON, H. (2004a). "Interactions Between Cavity Flow and Main Stream Skimming Flows: An Experimental Study". *Can. J. Civ. Engg.* 31(1), 33–44.
13. GONZALEZ, C.A. and CHANSON, H. (2004b). "Scale Effects in Moderate Slope Stepped Spillways. Experimental Studies in Air–Water Flows". *Proceedings of the 8th National Conference on Hydraulics in Water Engineering*, IEAust, Gold Coast, Australia, H. Chanson and J. Macintosh Ed., 8 pages (CD-ROM).
14. MATOS, J. (2001). "Onset of Skimming Flow on Stepped Spillways". Discussion *J. Hydraul. Engg. ASCE* 127(6), 519–521.
15. MOCHIZUKI, S., IZAWA, A. and OSAKA, H. (1996). "Turbulent Drag Reduction in a d-Type Rough Wall Boundary Layer with Longitudinal Thin Ribs Placed within Traverse Grooves Higher-Order Moments and Conditional Sampling Analysis". *Trans. JSME Intl Journal*, Series B, 39(3), 461–469.
16. MOSSA, M., YASUDA, Y. and CHANSON, H. (2004). Fluvial, Environmental and Coastal Developments in Hydraulic Engineering. Balkema, Leiden, The Netherlands, *Proceedings of the International Workshop on State-of-the-Art Hydraulic Engineering*, 16–19 Feb. Bari, Italy, 248 pp.
17. OHTSU, I., YASUDA, Y. and TAKAHASHI, M. (2004). "Flow Characteristics of Skimming Flows in Stepped Channels". *J. Hydraul. Engg. ASCE* 130(9), 860–869.
18. ORLANDI, P., LEONARDI, S. and ANTONIA, R.A. (2006). "Turbulent Channel Flow with Either Transverse or Longitudinal Roughness Elements on one Wall". *J. Fluid Mech.* 561, 279–305.
19. RAJARATNAM, N. (1990). "Skimming Flow in Stepped Spillways". *J. Hydraul. Engg. ASCE* 116(4), 587–591. Discussion: 118(1), 111–114.
20. TOOMBES, L. (2002). "Experimental Study of Air–Water Flow Properties on Low-Gradient Stepped Cascades". PhD Thesis, Department of Civil Engineering, The University of Queensland.
21. YASUDA, Y. and CHANSON, H. (2003). "Micro- and Macroscopic Study of Two-Phase Flow on a Stepped Chute". *Proceedings of the 30th IAHR Biennial Congress*, Thessaloniki, Greece, D695–D702.